Recovering of Silver from End-of-life Silicon Solar Panels Through a Peroxymonosulfate-based Advanced Oxidation Approach

Zhaoyi Yang[a], Longyan Chang,[b,c] Weijun Zhang,[d] Dongsheng Wang[*, e]

[a] Innovation Center of Yangtze River Delta, Zhejiang University, Jiaxing, 314100, Zhejiang, China

[b] Department of Environmental Science and Engineering, Xi'an Jiaotong University, Xi'an 710049, Shaanxi, China

[c] Qianjiang Water Resources Development Co, Zhejiang Hangzhou 310000, Zhejiang, China

[d] National Engineering Research Center of Industrial Wastewater Detoxication and Resource Recovery, Research Center for Eco-Environmental Sciences, Chinese Academy of Sciences, Beijing 100085, China

[e] Department of Environmental Engineering, Zhejiang University, Hangzhou 310058, Zhejiang, China

31 Pages

8 Texts

27 Figures

11 Tables

Table of contents

1. Supplementary Experimental Produces

Text 1. Chemicals.

Potassium peroxymonosulfate (PMS, $KHSO_5$•$0.5KHSO_4$•$0.5K_2SO_4$), Iron sulfate heptahydrate ($FeSO_4$·$7H_2O$), 5,5-dimethyl-1-pyrroline-N-oxide (DMPO), 2,2,6,6-tetramethyl-4-piperidinyloxyl (TEMP), *p*-benzoquinone (BQ), Methyl alcohol (MeOH), tert-butanol (TBA, AR), hydrochloric acid (HCl, 37%) were purchase from Sinopharm Chemical Reagent Co., Ltd. 9,10-diphenylanthracene (DPA), methyl phenyl sulfoxide (PMSO), and methyl phenyl sulfone ($PMSO_2$), Furfuryl alcohol (FFA) were obtained from Sigma. All chemicals were used as received without further purification. Deionized (DI) water with a resistivity of 18.2 MΩ•cm^{-1} was used throughout the experiments. Al-BSF Si cell, PERC Si cell, TOPCon Si cell, HIJ Si cell

and BC Si cell were purchased from Alibaba. The resins were purchased from Shanghai Kaiping Resin Co., Ltd.

Text 2. Dismantling of PV panels

The pyrolysis method was used to dismantle the EoL c-Si PV panels. The pyrolysis temperature was set at 500 °C and the holding time was 60 min. Materials including c-Si cells, glass, and solder strips were separated. 10% NaOH liquid was used to absorb the released HF during pyrolysis.

Text 3. Pretreatment of c-Si cells

The c-Si cells were first immersed in 18 wt% HCl for 1 h to remove the surface Al layer. The treated cells were then rinsed thoroughly with deionized water and dried at 70 ℃ under vacuum conditions for 12 h.

Text 4. DPA and $DPAO_2$ measurement

The 9,10-diphenylanthracene (DPA, 20 μM) was added into the PMS/Fe^{2+} system to oxidized. Reactions were conducted in 100 mL Teflon-lined screw-cap glass vials at 45℃. Acetonitrile (ACN, 50 mM) was added to ensure complete dissolution of DPA. At the reaction endpoint (20 min), an aliquot was withdrawn, filtered through a 0.22 μm PTFE membrane syringe filter to remove solid, and collected for analysis. Samples were analyzed using ultra-high-performance liquid chromatography coupled with quadrupole time-of-flight mass spectrometry (UHPLC-QTOF MS) equipped with an electrospray ionization (ESI) source operating in positive ionization mode. Chromatographic separation was performed on a Zorbax Eclipse Plus C8 column (2.1

× 150 mm, 1.7 μm particle size). The mobile phase comprised (A) acetonitrile and (B) Milli-Q water, applied with the following gradient program: initial composition 65:35 (v/v, A:B); increased linearly to 95:5 over 25 min; held at 95:5 for 10 min; ramped back to 65:35 in 0.5 min; maintained at 65:35 for 5 min for column re-equilibration. The mass spectrometer was operated with the following optimized parameters: scan type: full scan (MS1); resolution: 35,000 (defined at m/z 200); sheath gas flow rate: 20 units; auxiliary gas flow rate: 10 units; spray voltage: +3.0 kV; capillary temperature: 593.2 K.

Text 5. $PMS^{16}O^{16}O$ and $PMS^{16}O^{18}O$ measurement

For the determination of $^{18}O/^{16}O$ isotope-labelled $PMSO_2$, a Thermo Scientific Accucore aQ C18 column (2.1 × 150 mm, 2.6μm particle size) was employed. The column temperature was maintained at 40°C, the gradient mobile phase ratio of A/B was set as: the ratio kept at 90/10 for the first 5 min, then changed linearly from 90/10 to 10/90 in the next 15 min and held for 10 min, followed by a sharp decline to 90/10 in 0.1 min, and kept for 10 min for re-equilibration, where A is ultrapure water and B is acetonitrile with the flow rate of 0.50 mL/min. Accurate MS and MS/MS spectrums of $PMSO_2$ were analyzed in a parallel reaction monitoring (PRM) mode (m/z 50 to 500) in negative ESI mode.

Text 6. Electrochemical Tests

The electrochemical tests were performed by an Ivium-n-Stat workstation with a typical three-electrode setup. A platinum (Pt) plate (20 × 20 × 0.2 mm) and a $Hg/HgSO_4$

electrode (0.65 V vs standard hydrogen electrode, SHE) were applied as the counter electrode and reference electrode, respectively. The potential in this paper has been converted to the standard hydrogen electrode potential. Ti disk (φ= 5mm) was applied as the working electrode for chronoamperometry (CA) tests, as the Ti electrode shows poor electrocatalytic performance for hydrogen evolution reaction. For the electrodeposition experiments, Ti plates (20 × 20 × 0.2 mm) were used as the working and counter electrodes, respectively.

Text 7. Calculation of Energy Consumption and Chemical Inputs

In the recovery process of recovering Ag from c-Si cells with 10 cycles, the total chemicals consumption contained 1.75g PMS, 0.5427g $FeSO_4 \cdot 7H_2O$, 5g NaOH, and 50g H_2O. The c-Si cells were leached in a leaching reactor for 20 min at 45℃, and then electrodeposition for 120 min at 1.6 V. The liquid was then passed through an ion-exchange resin to remove sulphate ions and returned to the leaching reactor. Resin regeneration is carried out by immersing it in a 2.5% sodium hydroxide solution, and it is regenerated twice during the 10-cycle process. A total of 25g c-Si cells were processed in 10 cycles and the recovery Ag was calculated by the following formula eq (S1).

$$M = \sum_{i=0}^{10} m_i \tag{S1}$$

where M presents the total mass of recovered Ag, m_i represents the mass of Ag in the c-Si cells put into each cycle (g), The mass of recovered Ag calculated to be 231.4 mg.

The total energy consumption contains electricity utilization during the leaching process the electrodeposition. A power converter was used to calculate the power of the electrical heating and showed that it consumed 3 W when maintained a constant temperature of 45℃ during the leaching process. In the constant-voltage electrodeposition, the power of electrodeposition was 1.6 V × 0.005 A = 0.008 W. The energy consumption of the peristaltic pump during the resin adsorption process is 0.3 W. Therefore, the energy consumption during the 10 cycles was calculated as

$$\frac{3W \times 1200\ s \times 10 + 0.008W \times 7200\ s \times 10 + 0.2W \times 1200\ s \times 4}{3600000J/kW \cdot h} = 0.010\ kW \cdot h$$

The cost of chemical inputs of 1.75 g PMS, 0.5427 g $FeSO_4 \cdot 7H_2O$ (the cost of 50 g H_2O was negligible) could be calculated as

$$1.75g \times \frac{1.47}{1000} + 0.5427 \times \frac{0.08}{1000} + 5 \times \frac{0.28}{1000} = 0.004\ \$$$

Where PMS unit cost is 1.47 $\$\cdot kg^{-1}$, $FeSO_4 \cdot 7H_2O$ unit cost is 0.08 $\$\cdot kg^{-1}$, and NaOH unit cost is 0.28 $\$\cdot kg^{-1}$.

In total, 0.043 kW·h of energy and $0.017 in material consumption were utilized per gram of Ag recovered from c-Si cell.

Text 8. Life cycle assessment Analysis

The Life cycle assessment **(**LCA**)** of the Ag recycling process, along with their industrial production benchmarks, was conducted using SimaPro 9.3 software.

Background inventory data, including that relating to electricity, chemicals, and materials, was obtained from the Ecoinvent 3.5 database. This study quantified the environmental impacts associated with the recovery of 10 g Ag from EoL c-Si cells. The system boundary included raw material acquisition, transportation, production, and complete recycling operations, while excluding infrastructure construction as well as equipment manufacturing and maintenance. Eighteen impact categories were selected for analysis (see Tables S6–S9 for details). All assessments employed PERC c-Si solar cells as a standardized input to ensure comparability.

2. Supplementary Figures

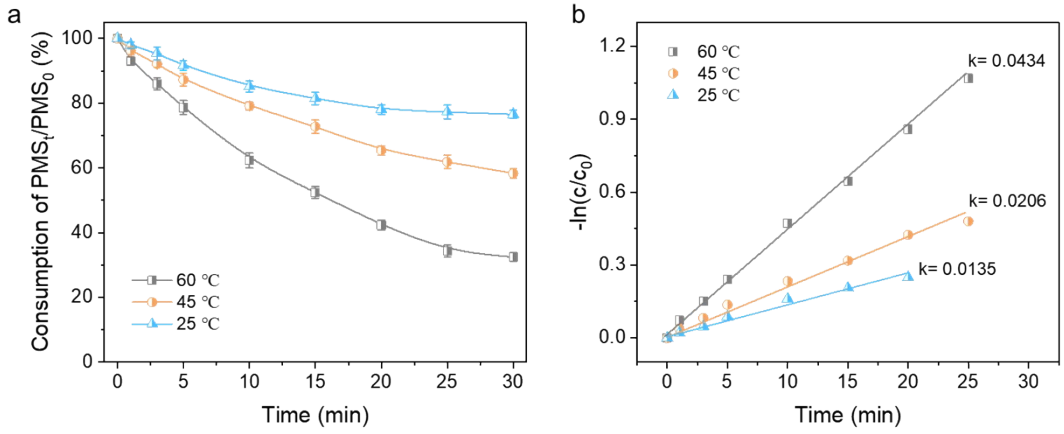

Figure S1. Comparison of decomposition ability of PMS by different temperature in PMS/Fe^{2+} system ($[PMS]_0$= 32.5 mM, $[Fe^{2+}]_0$= 6.5 mM, $[c\text{-Si-cells}]_0$= 2.5 g L^{-1}).

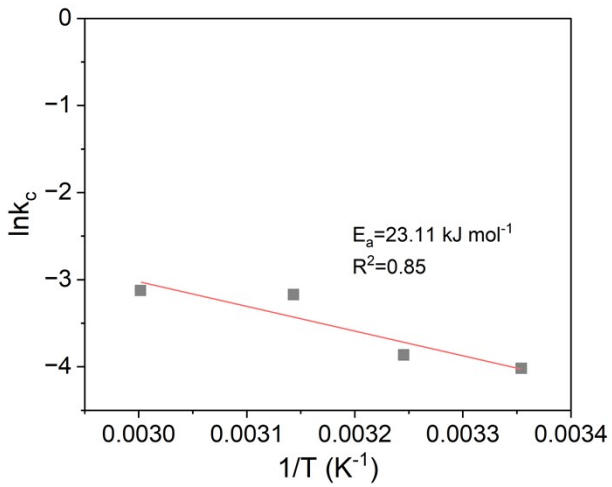

Figure S2. Arrhenius curves of Ag leaching.

Arrhenius equation which is shown as formula (S2):

$$k = Aexp\left(-\frac{E_a}{RT}\right) \quad \text{(S2)}$$

Where, k is the apparent rate constant, A is the pre-exponential, R is the molar gas constant (8.134 J·K^{-1}·mol^{-1}), T is the leaching temperature, in K.

Based on Equation (S2) and the reaction rate constants determined at different temperatures, the apparent activation energy for Ag leaching in the reaction system was calculated to be 23.11 kJ·mol^{-1}. The R^2 values obtained from the Arrhenius plots for Ag are relatively low. Since the Arrhenius equation assumes that the activation energy is independent of temperature, this observation suggests that the leaching mechanism of Ag is temperature-dependent. The deviation from the Arrhenius equation can be attributed to the fact that temperature directly affects the activation rate of PMS, thereby influencing the concentration of reactive species involved in Ag leaching.

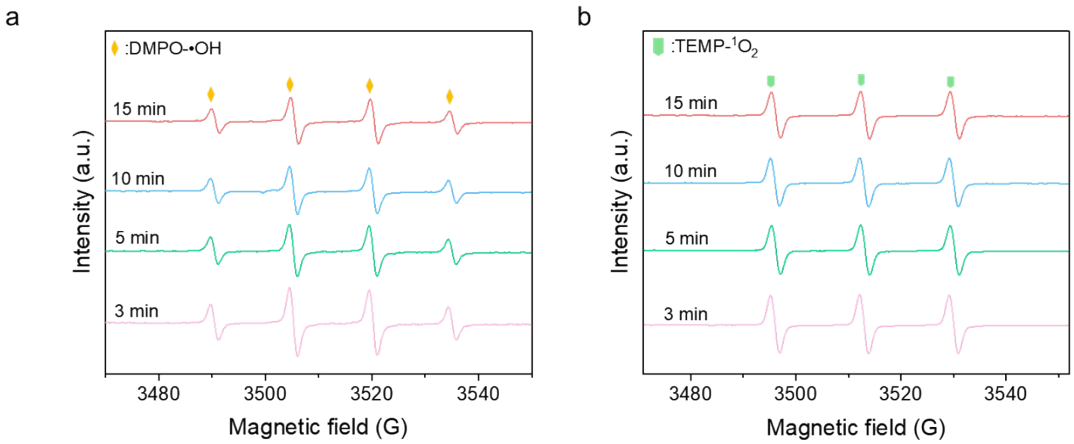

Figure S3. EPR spectra for the detection of the (a) DMPO-•OH and (b) TEMP-$^1O_2$ adduct in PMS+Fe^{2+} system.

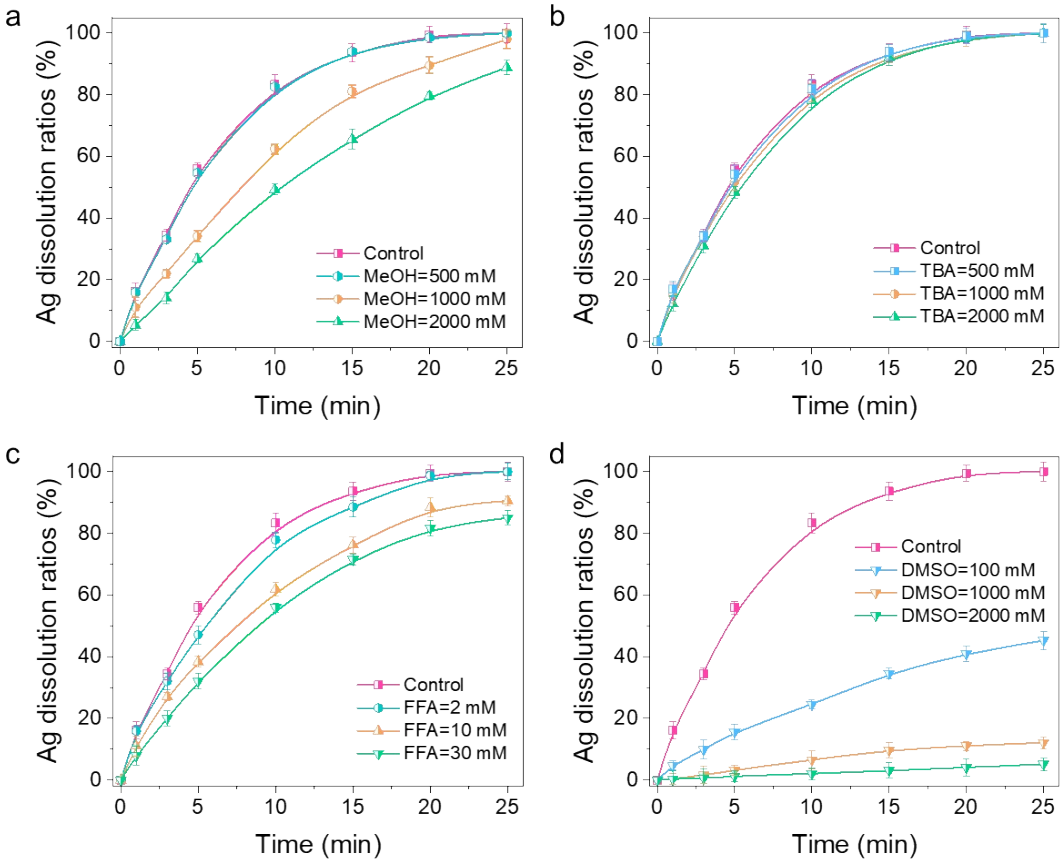

Figure S4. Dissolution ratios of Ag of c-Si cells in PMS/Fe^{2+} with different scavengers.

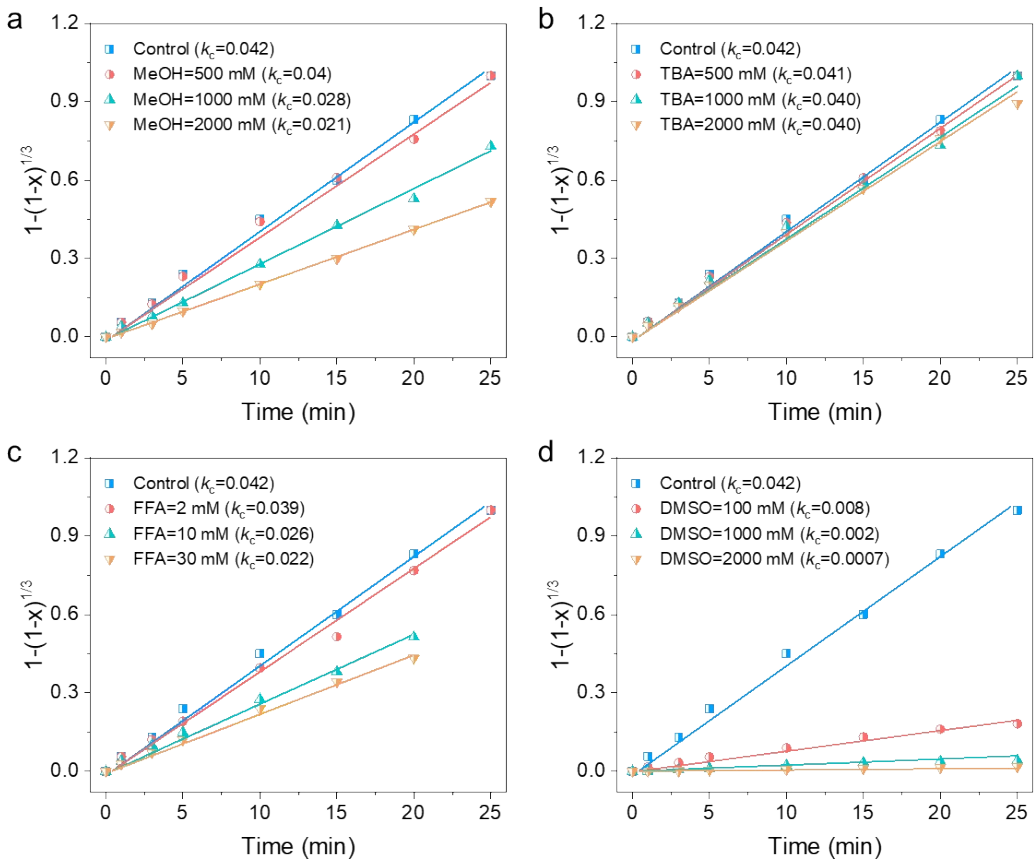

Figure S5. Reaction rate constant of Ag of c-Si cells in PMS/Fe^{2+} with different scavengers.

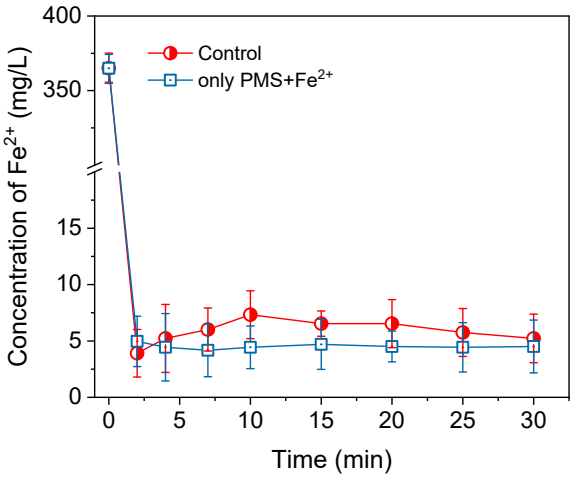

Figure S6. Concentration of Fe^{2+} for PMS/Fe^{2+} and c-Si cells/ PMS/Fe^{2+} systems.

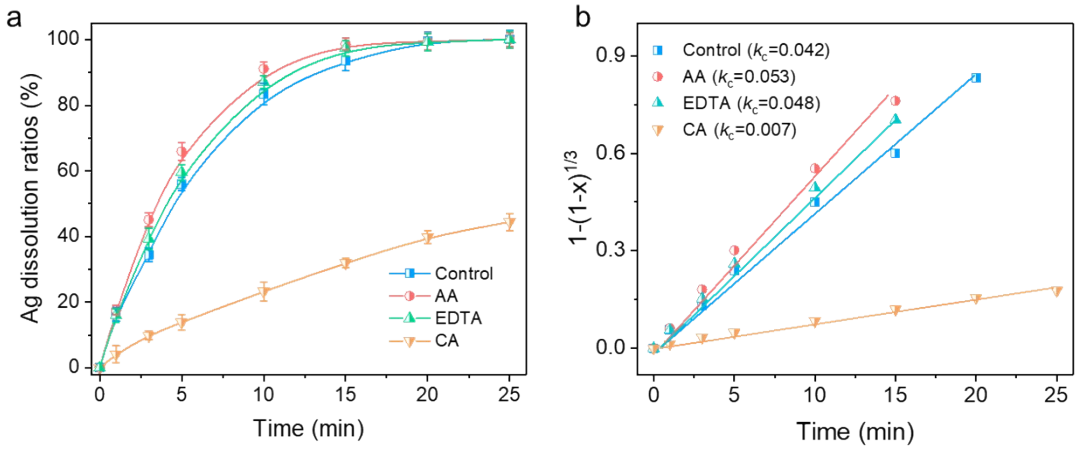

Figure S7. Dissolution ratios (a) and reaction rate constant (b) of Ag of c-Si cells in PMS/Fe^{2+} with different reducing agents and chelating agents added.

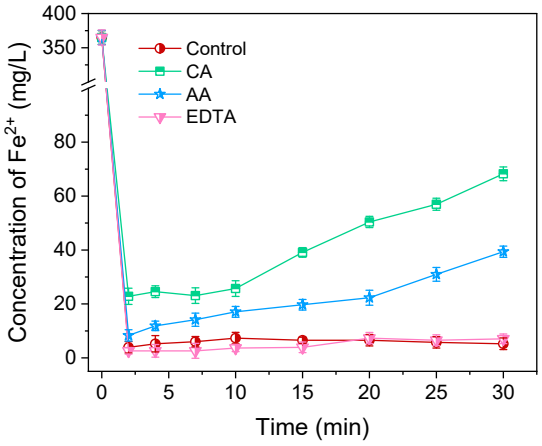

Figure S8. Concentration of Fe^{2+} for different reducing agents and chelating agents added.

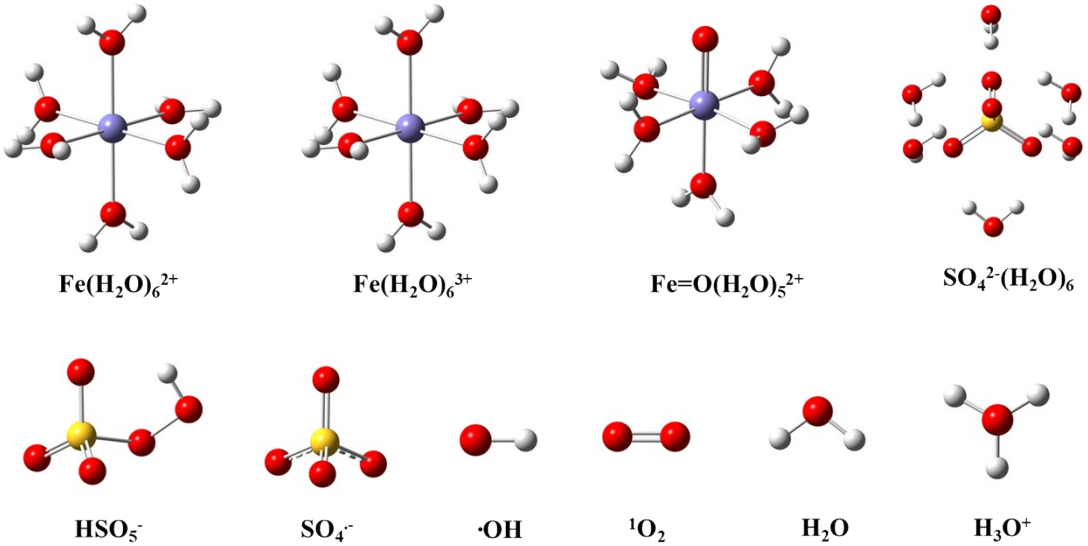

Figure S9. Model sketches of the optimized intermediates, transition state and products by DFT calculations.

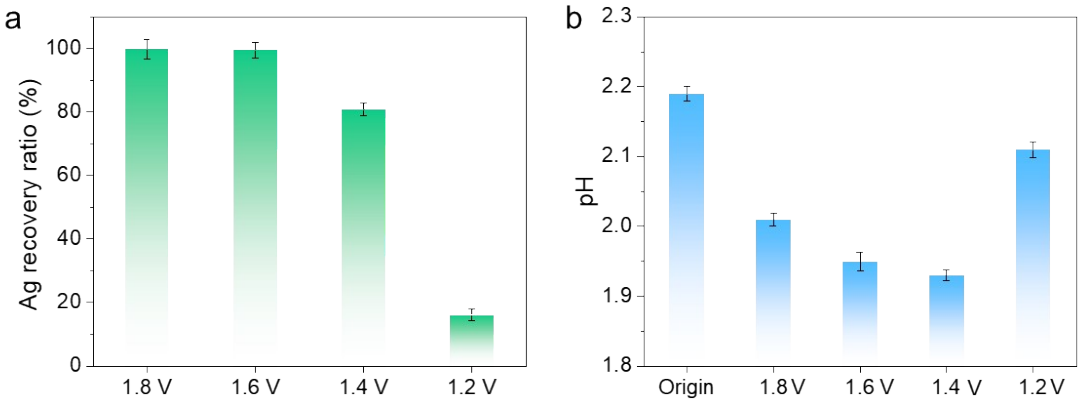

Figure S10. Ag recovery ratio (a) and pH value (b) under different potential.

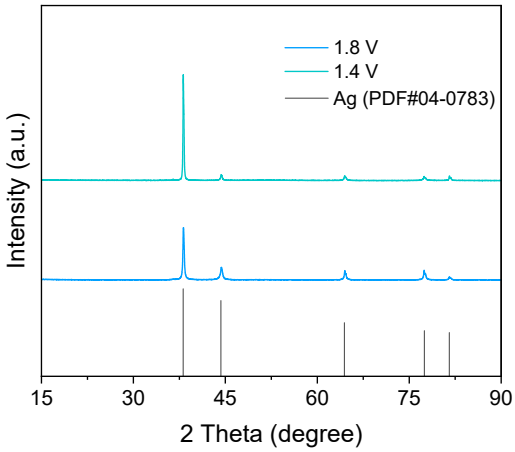

Figure S11. XRD patterns of Ag by-products during the electrodeposition process.

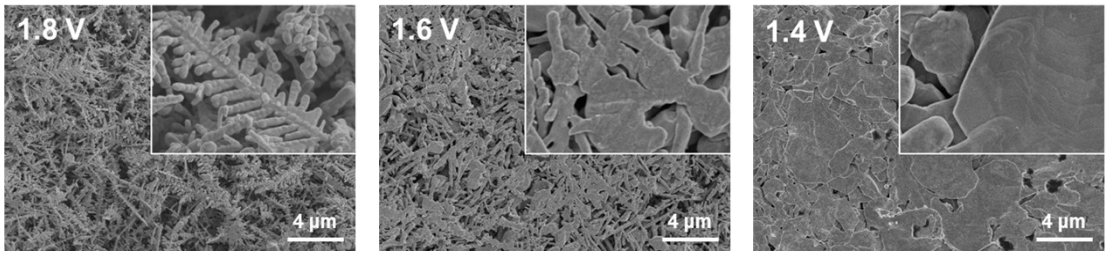

Figure S12. FESEM images of Ag electrodeposits under different potential (C_{Ag}= 350 ppm).

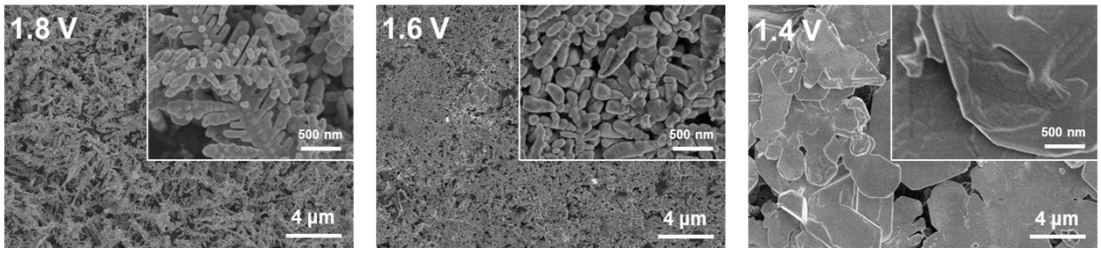

Figure S13. FESEM images of Ag electrodeposits under different potential (C_{Ag}= 695 ppm).

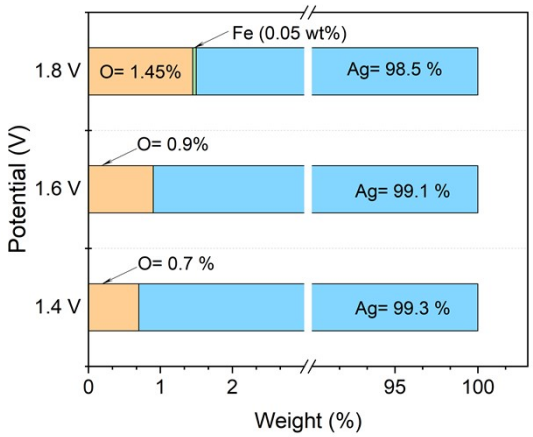

Figure S14. The surface chemical composition of Ag electrodeposits.

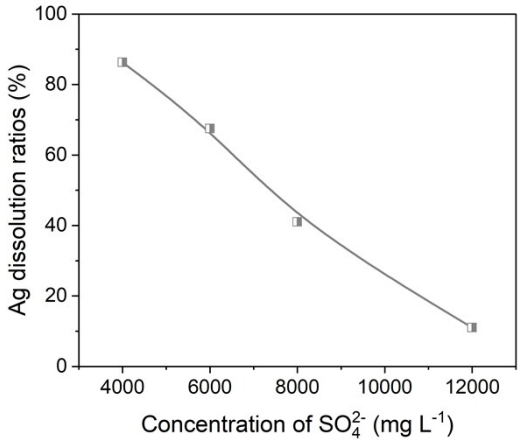

Figure S15. The effect of SO^{2-}_4 on Ag dissolution in PMS-Fe^{2+} system.

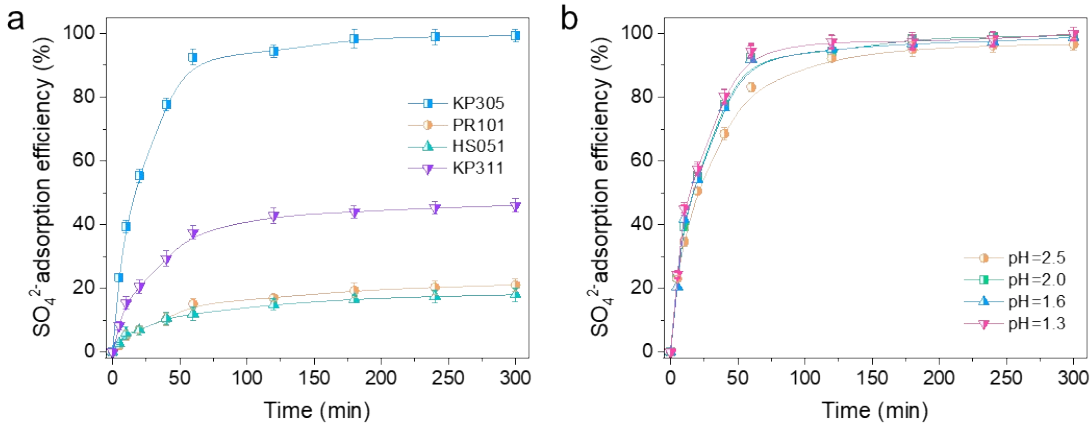

Figure S16. (a) Changes in the adsorption efficiency of different resins over time. (b) Effect of initial pH on SO^{2-}_4 adsorption ratios.

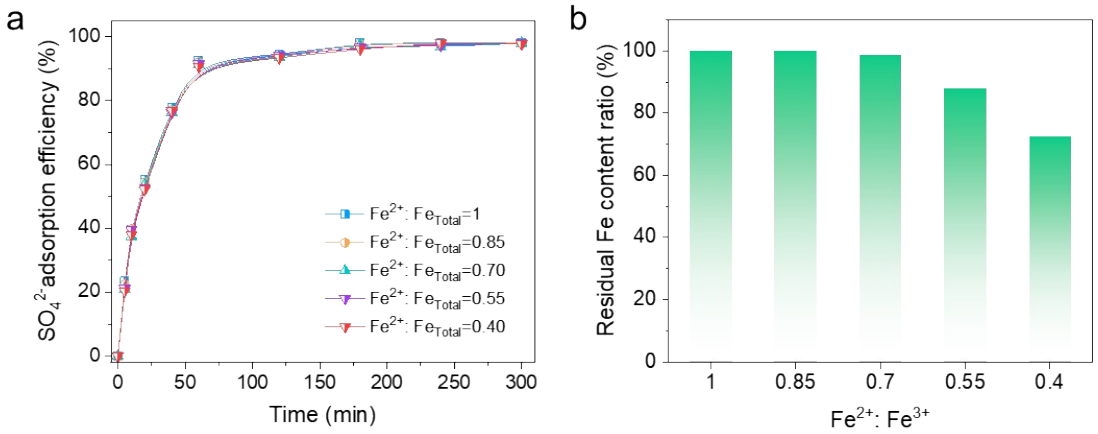

Figure S17. (a) Effect of initial Fe^{2+}/Fe_{Total} on SO_4^{2-} adsorption ratios. (b) Effect of the initial Fe^{2+}/Fe_{Total} on the iron content in the solution after adsorption.

Figure S18. The color of the resin after adsorption under different initials Fe^{2+}/Fe_{Total}.

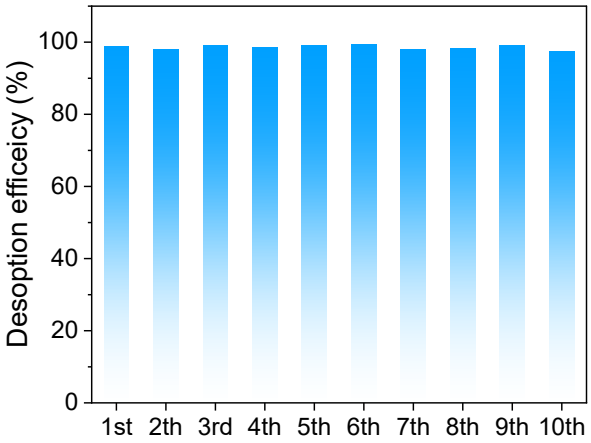

Figure S19. The cyclic desorption efficiency of the resin.

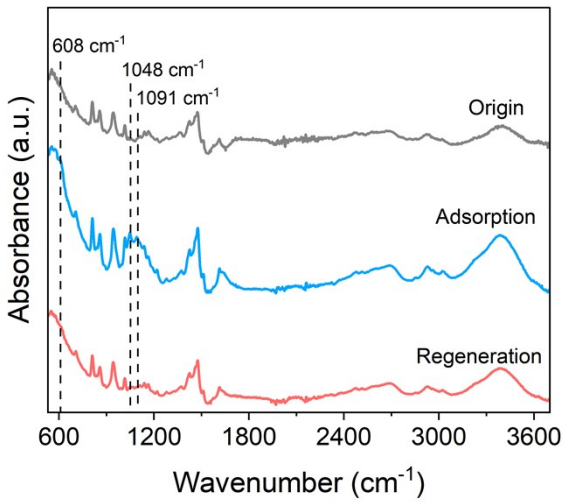

Figure S20. FT-IR spectra of the resin before and after absorption, and regeneration.

The absorption peaks at 608 cm^{-1} corresponds to the bending vibration of the O-S-O group of the SO_4^{2-}. The double peaks at 1048 and 1091 cm^{-1} represent the asymmetric stretching and symmetric stretching vibrations of SO_4^{2-}. As can be seen in Figure S19, after adsorption, the characteristic absorption peaks of SO_4^{2-} appeared on the resin at positions 608, 1048 and 1091 cm^{-1}. However, these absorption peaks disappeared after regeneration.

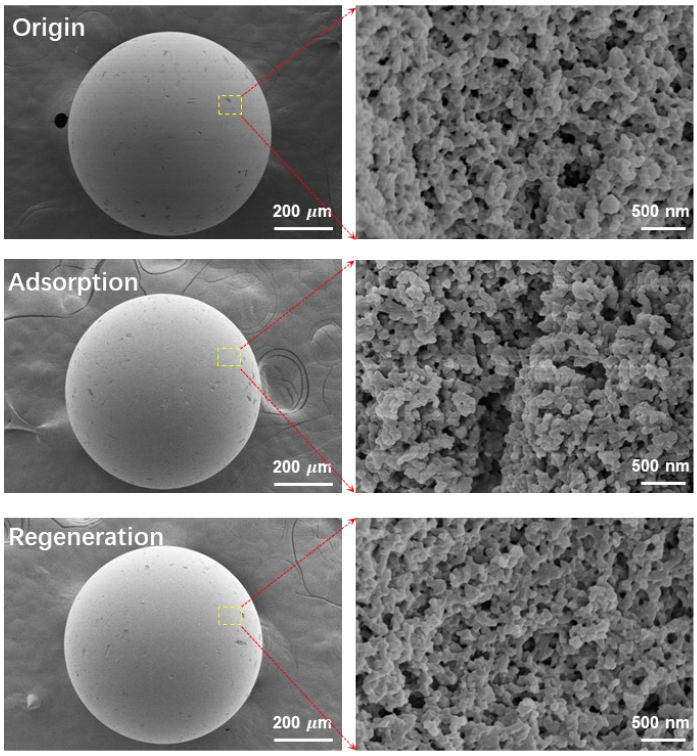

Figure S21. FESEM images of the resin before and after absorption, and after regeneration.

As can be seen in Figure S20, the resin is spherical particles with a diameter of 700 micrometers, and the interior has a porous structure. After the resin is adsorbed and regenerated, it still maintains its original morphological structure.

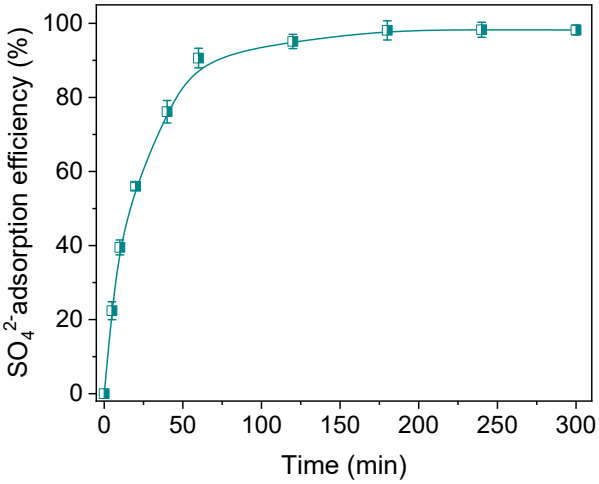

Figure S22. The static adsorption curve of sulfate removal by resin in the solution after electrodeposition.

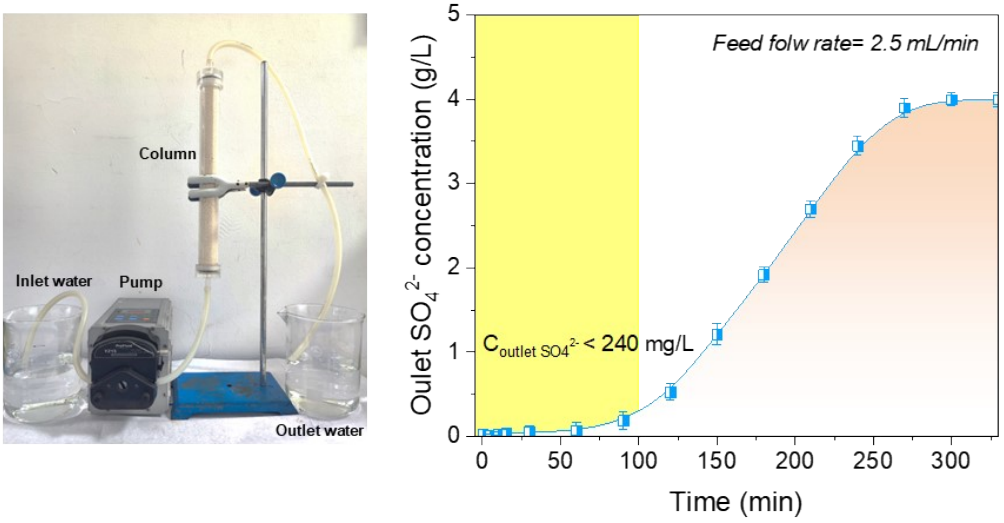

Figure S23. The dynamic adsorption curve of sulfate removal by resin in the solution after electrodeposition.

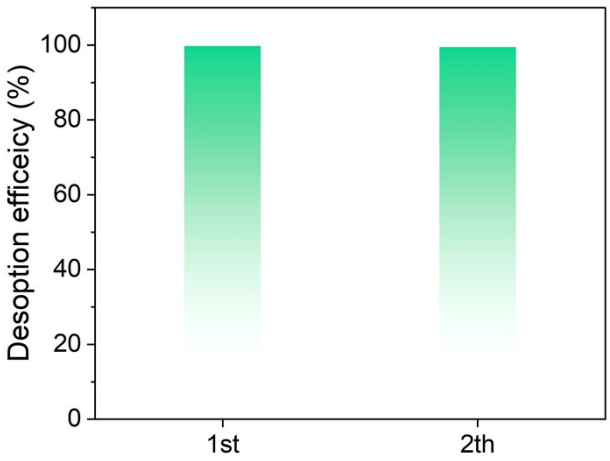

Figure S24. The cyclic desorption efficiency of the resin.

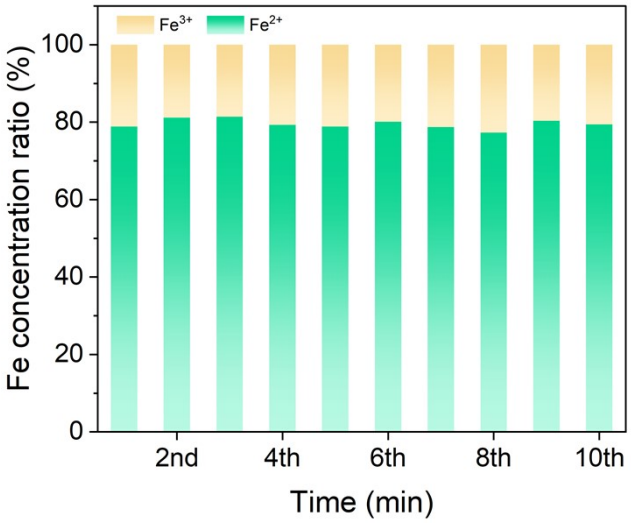

Figure S25. The proportion of Fe^{2+} and Fe^{3+} in the solution after electro-deposition during the recycling process.

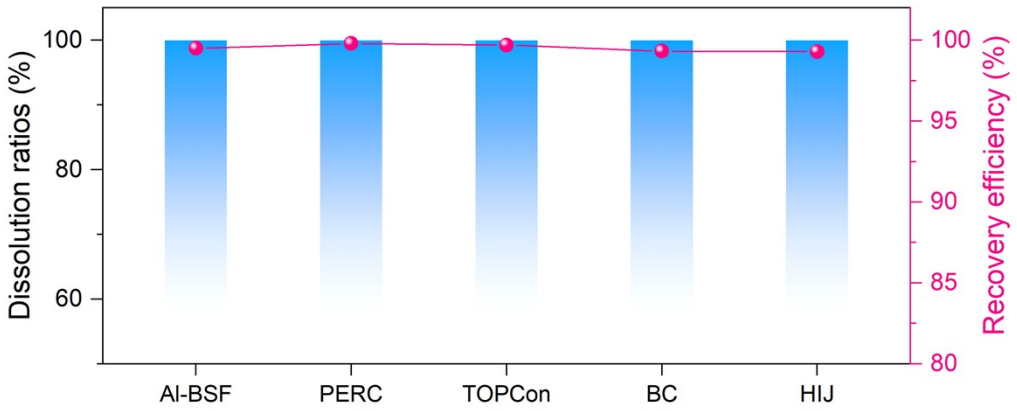

Figure S26. Testing of ag recovery in oxidation-electrodeposition integration process for different types of solar cells.

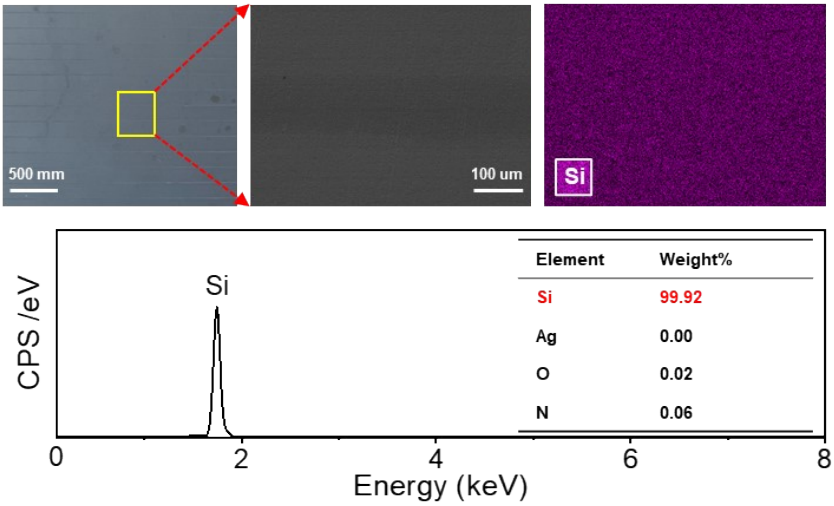

Figure S27. Digital picture, SEM images and EDS mapping of 5 wt% HF-treated solar cells.

After silver leaching in the PMS/Fe^{2+} system, the silicon nitride (Si_3N_4) layer on the surface of the solar cells remained intact. This layer can be effectively removed by treatment with hydrofluoric acid (HF), and the corresponding reaction equation is as follows:

$$Si_3N_4 + 22HF \rightarrow 3H_2SiF_6 + 4NH_4F \quad (1)$$

Experimental results indicate that the Si_3N_4 layer on the cell surface was completely removed after treatment with a 5% HF solution at room temperature for 1 hour (Figure S27). The experimental results can provide theoretical feasibility for the process development of further purification of silicon.

3. Supplementary Tables

Table S1. Content of Ag and Al in different types of c-Si cells.

	Al-BSF	PERC	TOPCon	HIJ	BC
Ag (wt%)	0.71	0.93	0.62	1.31	0.54
Al (wt%)	4.81	2.17	1.81	0.43	0.73

Table S2. The summary of the total Gibbs free energy (G_{total}), the correction of Gibbs free energy (G_{corr}), and the single point energy (E_{sp}) for eqs. 2-5.

	ΔG_{total} (eV)	G_{corr} (a.u.)	E_{sp} (vacuum, a.u.)	G_{total} (a.u.)
$Fe(H_2O)_6^{2+}$		0.1052	-1722.1998	-1722.0906
HSO_5^-		0.0031	-775.0296	-775.0266
$SO_4^{\cdot -}$	-0.95	-0.0130	-699.2173	-699.2303
$Fe(H_2O)_6^{3+}$		0.1146	-1721.9996	-1721.9751
OH^-		-0.0077	-75.9390	-75.9467
$SO_4^{\cdot -}$		-0.0130	-699.2173	-699.2303
H_2O		0.0032	-76.4393	-76.4361
$SO_4^{2-}(H_2O)_6$	-0.81	0.1134	-1158.1318	-1158.1614
H_3O^+		0.0152	-76.8533	-76.8381
$\cdot OH$		-0.0083	-75.7409	-75.7493
$Fe(H_2O)_6^{2+}$		0.1052	-1722.1998	-1722.0946
HSO_5^-		0.0031	-775.0296	-775.0266
H_2O		0.0032	-76.4393	-76.4361
$Fe=O(H_2O)_5^{2+}$	-0.06	0.0943	-1720.7906	-1720.7404
$SO_4^{2-}(H_2O)_6$		0.1134	-1158.1318	-1158.1614
H_3O^+		0.0152	-76.8533	-76.8381
$Fe=O(H_2O)_5^{2+}$		0.0943	-1720.7906	-1720.7404
HSO_5^-		0.0031	-775.0296	-775.0266
H_2O	-2.45	0.0032	-76.4393	-76.4361
$Fe(H_2O)_6^{2+}$		0.1052	-1722.1998	-1722.0906
$^1O_2$		-0.0149	-150.2706	-150.2555

$SO_4^{2-}(H_2O)_6$	0.1134	-1158.1318	-1158.1614
H_3O^+	0.0152	-76.8533	-76.8381

Note: G_{corr} refers to the correction of Gibbs free energy; Esp means the single point energy; G_{total} refers to the total Gibbs free energy.

Table S3. Comparison of this work with other methods in Ag recovery reaction reported in literature

Methods	**Treatment**	**Energy consumption kWh·(Ag g)$^{-1}$**	**Chemicals consumption $·(Ag g)$^{-1}$**	**Secondary waste**	**Ref**
I_2-KI	Leaching (25℃, 20min)	0.097	0.94	I_2	[1]
Citric acid+H_2O_2	Leaching (25℃, 2.5h)	0.41	0.073	Citric acid /NH_3	[2]
ChCl·4H_2O/$FeCl_3$	Leaching (25℃, 10 min)	0.45	2.19	Fe^{3+}	[3]
$CaCl_2$·6H_2O/$FeCl_3$	Leaching (65℃, 10 min)	0.88	0.183	Fe^{3+}	[3]
HNO_3	Leaching (25℃, 2h)	0.37	0.47	HNO_3/NO_x	[4]
NaOH-KOH	Leaching (200℃, 20s)	0.87	0.032	Na_2SiO_3/$NaAlO_2$	[5]
NH_4SCN/$Fe_2(SO_4)_3$/lignin	Leaching (120℃, 3h)	2.19	0.91	NH_4SCN/ $Fe_2(SO_4)_3$	[6]
$Na_2S_2O_3$/Cu^{2+}	Leaching (60℃, 0.5h)	0.53	0.20	$Na_2S_2O_3$/Cu^{2+}	[7]
CH_3CN/$BaTiO_3$	Piezocatalytic leaching (20 h)	0.052	1.54	CH_3CN	[8]
CH_3CN/TiO_2	Photocatalyst leaching (24 h)	147	3.0	CH_3CN	[9]
Polyiodide ionic liquids $[N_{1888}]$ $[I_3]$	Leaching (55℃, 3h)	0.072	0.065	Ethanol/NaI	[10]
PMS/Fe^{2+}	Leaching (45℃, 20min)	0.044	0.011	SO_4^{2-}	This work

Table S4. Inputs and outputs of scenario 1.

Inputs/Outputs	Quantity	Units
Step1:		
Inputs		
c-Si cells	1109.88	g
HNO_3	1465.04	g
H_2O	1864.60	g
Electricity	0.19	kw.h
Outputs		
c-Si cells	1099.56	g
$AgNO_3$ solution	3335.55	g
Toxic NO_2 gas	4.41	g
Step2:		
Inputs		
$AgNO_3$ solution	3335.55	g
NaOH	665.93	g
H_2O	998.89	g
Electricity	0.20	kw.h
Outputs		
Ag_2O	10.77	g
Wastes chemical	4989.60	g
TN	219.76	g
Step3:		
Inputs		
Ag_2O	10.77	g
Electricity	4.88	kw.h
Outputs		
Ag	10.00	g
O_2	0.78	g

Table S5. Inputs and outputs of scenario 2.

Inputs/Outputs	Quantity	Units
Step1+Step2:		
Inputs		
c-Si cells	1080.38	g
PMS	73.88	g

$FeSO_4 \cdot 7H_2O$	23.45	g
H_2O	21.61	g
Electricity	0.42	kw.h
Outputs		
c-Si cells	1070.38	g
Ag	10.00	g
SO_4^{2-} solution	118.94	g
Step3:		
Inputs		
SO_4^{2-} solution	118.94	g
NaOH	21.61	g
H_2O	864.30	g
Electricity	0.01	kw.h
Outputs		
Wastes chemical	1004.84	g

Table S6. The environmental impacts of this method in scenario 1 on the basis of recycling 10 g Ag from c-Si cells.

Impact category	Unit	Total	Step1	Step2	Step3
Global warming	kg CO_2 eq	4.963202	5.413768	1.041064	-1.491629
Stratospheric ozone depletion	kg CFC11 eq	0.000090	0.000094	0.000001	-0.000005
Ionizing radiation	kBq Co-60 eq	0.375904	0.283501	0.115577	-0.023175
Ozone formation, Human health	kg NO_x eq	-0.017670	0.016113	0.002652	-0.036434
Fine particulate matter formation	kg $PM_{2.5}$ eq	0.002681	0.008678	0.002327	-0.008324
Ozone formation, Terrestrial ecosystems	kg NO_x eq	-0.018007	0.016280	0.002678	-0.036965
Terrestrial acidification	kg SO_2 eq	0.002001	0.021497	0.003989	-0.023484
Freshwater eutrophication	kg P eq	-0.011786	0.001436	0.000539	-0.013761
Marine eutrophication	kg N eq	0.065307	0.000129	0.065347	-0.000169
Terrestrial ecotoxicity	kg 1,4-DCB	-17.510175	11.059107	3.890223	-32.459506
Freshwater ecotoxicity	kg 1,4-DCB	-9.637435	0.199062	0.071942	-9.908438
Marine ecotoxicity	kg 1,4-DCB	-15.508262	0.261133	0.093061	-15.862457
Human carcinogenic toxicity	kg 1,4-DCB	0.136834	0.490549	0.049150	-0.402865
Human non-carcinogenic toxicity	kg 1,4-DCB	-153.861914	4.792754	1.354934	-160.009602
Land use	m^2a crop eq	-0.323337	0.052101	0.022969	-0.398407
Mineral resource scarcity	kg Cu eq	-1.474341	0.032897	0.003883	-1.511120
Fossil resource scarcity	kg oil eq	0.647679	0.840134	0.258210	-0.450665
Water consumption	m^3	1.897163	1.888215	0.020576	-0.011628

Table S7. The environmental impacts of this method in scenario 2 on the basis of recycling 10 g Ag from c-Si cells.

Impact category	Unit	Total	Step1+Step2	Step3
Global warming	kg CO_2 eq	-4.256151	-4.300418	0.044267
Stratospheric ozone depletion	kg CFC11 eq	-0.000003	-0.000003	0.000000
Ionizing radiation	kBq Co-60 eq	-0.398522	-0.401504	0.002982
Ozone formation, Human health	kg NO_x eq	-0.037624	-0.037740	0.000115
Fine particulate matter formation	kg $PM_{2.5}$ eq	-0.013163	-0.013245	0.000082
Ozone formation, Terrestrial ecosystems	kg NO_x eq	-0.038367	-0.038484	0.000118
Terrestrial acidification	kg SO_2 eq	-0.030088	-0.030243	0.000154
Freshwater eutrophication	kg P eq	-0.012862	-0.012879	0.000017
Marine eutrophication	kg N eq	-0.000265	-0.000272	0.000007
Terrestrial ecotoxicity	kg 1,4-DCB	-46.090789	-46.383272	0.292483
Freshwater ecotoxicity	kg 1,4-DCB	-9.947982	-9.949911	0.001929
Marine ecotoxicity	kg 1,4-DCB	-13.624658	-13.627429	0.002771
Human carcinogenic toxicity	kg 1,4-DCB	-0.994221	-1.003541	0.009320
Human non-carcinogenic toxicity	kg 1,4-DCB	-144.935989	-144.989167	0.053178
Land use	m^2a crop eq	-0.386422	-0.387203	0.000781
Mineral resource scarcity	kg Cu eq	-0.778750	-0.782390	0.003640
Fossil resource scarcity	kg oil eq	-1.129709	-1.140135	0.010426
Water consumption	m^3	-0.030154	-0.030542	0.000388

Table S8. The environmental impacts of cumulative energy demand in scenario 1 on the basis of recycling 10 g Ag from c-Si cells.

Impact category	Unit	Total	Step1	Step2	Step3
Total	MJ	41.53139	46.99984	15.4755	-20.944
Non-renewable, fossil	MJ	29.690175	38.445946	11.852836	-20.608607
Non-renewable, nuclear	MJ	7.069107	5.300187	2.134892	-0.365971
Non-renewable, biomass	MJ	0.001984	0.001069	0.000383	0.000531
Renewable, biomass	MJ	0.624578	0.687769	0.304974	-0.368164
Renewable, wind, solar, geothe	MJ	1.219983	0.605025	0.272157	0.342801
Renewable, water	MJ	2.925558	1.959847	0.910253	0.055458

Table S9. The environmental impacts of cumulative energy demand in scenario 2 on the basis of recycling 10 g Ag from c-Si cells.

Impact category	Unit	Total	Step1+Step2	Step3
Total	MJ	-65.26922532	-65.8572488	0.588023479
Non-renewable, fossil	MJ	-52.24870492	-52.72909007	0.48038515
Non-renewable, nuclear	MJ	-7.416310304	-7.471671603	0.055361298
Non-renewable, biomass	MJ	-0.000694396	-0.000729402	3.50058E-05
Renewable, biomass	MJ	-0.980223672	-0.989135388	0.008911716
Renewable, wind, solar, geothe	MJ	-1.653704721	-1.669143395	0.015438674

Renewable, water	MJ	-2.969587312	-2.997478946	0.027891634

Table S10. Cost and benefit analysis of scenario 1.

Feedstock costs			
Name	Consumption (kg/kg Ag)	Unit price ($/kg)	Operation costs ($/kg Ag)
HNO_3 (68%)	146.504	0.205	30.03
NaOH	66.593	0.7	46.62
Waste liquid treatment	498.96	0.25	124.74
Electricity costs			
Name	Consumption (kw.h/kg Ag)	Unit price ($/kw.h)	Operation costs ($/kg Ag)
Electricity costs	527	0.0952	50.17
Special dividends			
Name	Consumption (kg)	Unit price ($/kg)	
Ag	1	820	820
Cost of purchasing EoL c-Si cells			
Name	Consumption (kg)	Unit price ($/kg)	
EoL c-Si cells	110.988	3.49	386.99
The total profits			
The total profits= special dividends -feedstock costs -electricity costs -cost of purchasing EoL c-Si cells =820-201.39-50.17-386.99=181.45			

Table S11. Cost and benefit analysis of scenario 2.

Feedstock costs			
Name	Consumption (kg/kg Ag)	Unit price ($/kg)	Operation costs ($/kg Ag)

PMS	7.39	1.47	10.86
$FeSO_4 \cdot 7H_2O$	2.35	0.08	0.19
NaOH	2.16	0.28	0.61
Waste liquid treatment	100.48	0.25	25.12
Electricity costs			
Name	Consumption (kw.h/kg Ag)	Unit price ($/kw.h)	Operation costs ($/kg Ag)
Electricity costs	43	0.0952	4.09
Special dividends			
Name	Consumption (kg)	Unit price ($/kg)	
Ag	1	820	820
Cost of purchasing EoL c-Si cells			
Name	Consumption (kg)	Unit price ($/kg)	
EoL c-Si cells	108.038	3.49	376.70
The total profits			
The total profits= special dividends -feedstock costs -electricity costs -cost of purchasing EoL c-Si cells =820-36.77-4.09-376.70=402.43			

4. References

1. Chung, J.; Seo, B.; Lee, J.; Kim, J. Y., Comparative analysis of I2-KI and HNO3 leaching in a life cycle perspective: Towards sustainable recycling of end-of-life c-Si PV panel. *Journal of Hazardous Materials* **2021,** *404*.
2. Zheng, R.; Luo, M.; Li, B.; Jia, M.; Zhang, H.; Liu, S.; Lu, Y.; Jiang, L.; Zhang, Z.; Liu, F., Eco-friendly recovery and preparation of high purity nano silver powders from retired photovoltaic solar cells. *Separation and Purification Technology* **2025,** *359*.
3. Zante, G.; Marin Rivera, R.; Hartley, J. M.; Abbott, A. P., Efficient recycling of metals from solar cells using catalytic etchants. *Journal of Cleaner Production* **2022,** *370*.
4. Ding, Y.; He, J.; Zhang, S.; Jian, J.; Shi, Z.; Cao, A., Efficient and comprehensive recycling of valuable components from scrapped Si-based photovoltaic panels. *Waste Management* **2024,** *175*, 183-190.

5. Gao, S.; Chen, X.; Qu, J.; Guo, Y.; Shi, H.; Pang, F.; Guo, L.; Qu, X.; Wang, D.; Yin, H., Recycling of silicon solar panels through a salt-etching approach. *Nature Sustainability* **2024,** *7* (7), 920-930.
6. Yang, S.; Chen, G.; Cai, Y.; Guo, H.; Yao, W.; Tang, M., Selective leaching of silver-rich residue in NH4SCN solution under oxygen pressure. *Separation and Purification Technology* **2011,** *77* (1), 1-6.
7. Zhang, Z. Y.; Wu, L.; He, K.; Zhang, F. S., A sequential leaching procedure for efficient recovery of gold and silver from waste mobile phone printed circuit boards. *Waste Management* **2022,** *153*, 13-19.
8. Zhou, D.; Li, Z.; Chen, Y.; Dong, H.; Zhou, Y.; Bian, Z.; Zhu, M., Leveraging Solvent Effects for Enhanced Oxidation and Coordination in Selective Piezocatalytic Gold Recovery from End-of-Life Electronics. *Angew Chem Int Ed Engl* **2025**, e202502751.
9. Chen, Y.; Xu, M.; Wen, J.; Wan, Y.; Zhao, Q.; Cao, X.; Ding, Y.; Wang, Z. L.; Li, H.; Bian, Z., Selective recovery of precious metals through photocatalysis. *Nature Sustainability* **2021,** *4* (7), 618-626.
10. Yin, X.; Wang, S.; Liu, R.; Liu, X.; Liu, P.; Yang, Y., New and facile recovery strategy for silver, copper, and nickel from waste silver contacts using polyiodide ionic liquids. *AIChE Journal* **2024,** *70* (7).